

AD A 042599

# Measurement of Solid Friction Parameters of Ball Bearings

Engineering Science Operations  
The Aerospace Corporation  
El Segundo, Calif. 90245

10 March 1977

Interim Report

APPROVED FOR PUBLIC RELEASE:  
DISTRIBUTION UNLIMITED

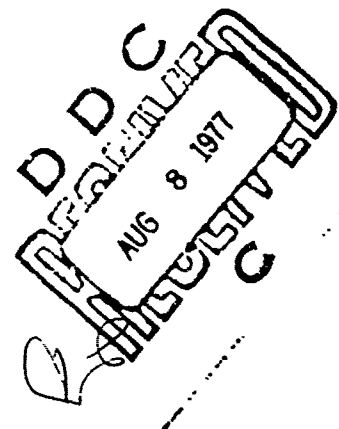
Prepared by  
SPACE AND MISSILE SYSTEMS ORGANIZATION  
AIR FORCE SYSTEMS COMMAND  
Los Angeles Air Force Station  
P.O. Box 92960, Worldway Postal Center  
Los Angeles, Calif. 90009



THE AEROSPACE CORPORATION

AD NO. \_\_\_\_\_  
DDC FILE COPY


12




This interim report was submitted by The Aerospace Corporation, El Segundo, CA 90245, under Contract F04701-76-C-0077 with the Space and Missile Systems Organization (AFSC), Los Angeles Air Force Station, P. O. Box 92960, Worldway Postal Center, Los Angeles, CA 90009. It was reviewed and approved for The Aerospace Corporation by D. J. Griep, Engineering Science Operations. First Lieutenant A. G. Fernandez, YAPT, was the Deputy for Advanced Space Programs project engineer.


This report has been reviewed by the Information Office (OI) and is releasable to the National Technical Information Service (NTIS). At NTIS, it will be available to the general public, including foreign nations.

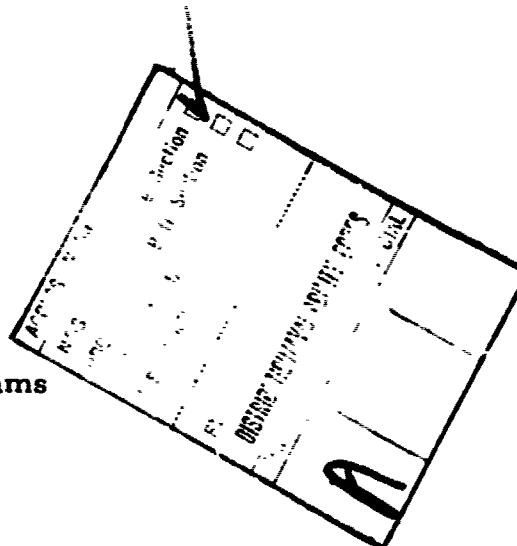
This technical report has been reviewed and is approved for publication. Publication of this report does not constitute Air Force approval of the report's findings or conclusions. It is published only for the exchange and stimulation of ideas.

  
A. G. Fernandez, 1st Lt, USAF  
Project Engineer

  
Joseph Gassmann, Maj, USAF

FOR THE COMMANDER

  
Leonard E. Baltzell, Col, USAF  
Asst. Deputy for Advanced Space Programs



UNCLASSIFIED

SECURITY CLASSIFICATION OF THIS PAGE (When Data Entered)

REPORT DOCUMENTATION PAGE		READ INSTRUCTIONS BEFORE COMPLETING FORM
1. REPORT NUMBER <b>SAMSO-TR-77-132</b>	2. GOVT ACCESSION NO. <b>TR-77-132</b>	3. RECIPIENT'S CATALOG NUMBER
4. TITLE (and Subtitle) <b>MEASUREMENT OF SOLID FRICTION PARAMETERS OF BALL BEARINGS.</b>		5. TYPE OF REPORT & PERIOD COVERED <b>Interim</b>
7. AUTHOR(s) <b>Phil R. Dahl</b>		6. PERFORMING ORG. REPORT NUMBER <b>TR-0077(2901-03)-3</b>
9. PERFORMING ORGANIZATION NAME AND ADDRESS <b>The Aerospace Corporation El Segundo, CA 90009</b>		8. CONTRACT OR GRANT NUMBER(s) <b>F04701-76-C-0077</b>
11. CONTROLLING OFFICE NAME AND ADDRESS <b>Space and Missile Systems Organization/YAPT P.O. Box 92960, Worldway Postal Center Los Angeles, CA 90009</b>		10. PROGRAM ELEMENT, PROJECT, TASK AREA & WORK UNIT NUMBERS
14. MONITORING AGENCY NAME & ADDRESS (if different from Controlling Office)		12. REPORT DATE <b>10 Mar 1977</b>
		13. NUMBER OF PAGES <b>25 p.</b>
		15. SECURITY CLASS. (of this report) <b>Unclassified</b>
		15a. DECLASSIFICATION/DOWNGRADING SCHEDULE
16. DISTRIBUTION STATEMENT (of this Report)  <b>Approved for public release; distribution unlimited.</b>		
17. DISTRIBUTION STATEMENT (of the abstract entered in Block 20, if different from Report)		
18. SUPPLEMENTARY NOTES		
19. KEY WORDS (Continue on reverse side if necessary and identify by block number) <b>Solid Friction Ball Bearing Friction Friction Measurement Friction Parameters</b>		
20. ABSTRACT (Continue on reverse side if necessary and identify by block number) <b>The near static friction behavior of ball bearings and other devices can be described by the author's mathematical model of solid friction. Three or more parameters used in the model need to be defined for a particular bearing that may be employed in a motor/load system design. At present, little or no data are available to define these parameters, and there is also little or no information on the subject of test methods for obtaining solid friction model parameter data. This paper presents the results of some tests performed to</b>		

UNCLASSIFIED

SECURITY CLASSIFICATION OF THIS PAGE(When Data Entered)

19 F. WORDS (Continued)

20 ABSTRACT (Continued)

measure the solid friction parameters of ball bearings. The test method is described, and typical test data are shown. The method of data reduction is based on the analytical quasi-static model and is described in some detail.

Friction model parameter results are presented for a 2-1/2 in. OD duplex bearing pair with preloads in the range from 6 to 36 lb.



UNCLASSIFIED

## PREFACE

I wish to express my appreciation to Tom Wheelock of the Bendix Corporation for his interest and assistance in the testing effort. The assistance of Murry Ashcraft and Don Werhan in the experiments is also gratefully acknowledged.

## CONTENTS

I.	INTRODUCTION .....	5
II.	SOLID FRICTION MODEL PARAMETERS .....	5
III.	TEST METHOD .....	6
	Bearing Test Fixture .....	7
	Torque Meter .....	7
	Drive Servo .....	7
IV.	DATA ANALYSIS .....	8
V.	RESULTS AND CONCLUSIONS .....	9
	REFERENCES .....	9

## FIGURES

1.	Motor/Gear Box/Load System . . . . .	10
2.	System Diagram . . . . .	11
3.	Solid Friction Behavior . . . . .	12
4.	Gear-Shaft Stiffness with Hysteresis (as Measured at Output Shaft) . . . . .	12
5.	Friction Slope Model for Gear-Shaft Stiffness, Hysteresis, and Backlash . . . . .	13
6.	Gear-Shaft Stiffness with Hysteresis and Backlash . . . . .	14
7.	Friction Slope Functions . . . . .	15
8.	Force Deflection Hysteresis Loops . . . . .	16
9.	Bearing Static Torque-Deflection Test Setup . . . . .	17
10.	Old Bearing Hysteresis Loop . . . . .	18
11.	New Bearing Hysteresis Loop . . . . .	19
12.	Running Friction versus Preload . . . . .	20

## TABLES

I.	Drive Servo Range and Resolution . . . . .	21
II.	Bearing Pair SFM Parameters . . . . .	22

# MEASUREMENT OF SOLID FRICTION PARAMETERS OF BALL BEARINGS

P. R. Dahl

The Aerospace Corporation  
El Segundo, California

## I. INTRODUCTION

A schematic of an electric motor gearbox and inertia load is shown in Figure 1. The system block diagram can be depicted as in Figure 2 where the electrically generated torque  $T_E$  drives the motor inertia which, in turn, applies torque through the gearbox to the load inertia. The motor electromechanical characteristics such as back EMF and torque constant are not shown in this diagram. Three forms of friction are present: viscous friction, solid friction, and magnetic hysteresis "friction." The first form, viscous friction, is so familiar it needs no description here. The second form is commonly called Coulomb friction or "stiction," and is referred to in this paper as Solid Friction or SF. A solid friction model (SFM) that aptly describes this type of rolling friction was devised recently [1, 2, 3]. It has the appearance shown in Figure 3 and will be described later in this discussion. The third form is a hysteretic drag torque produced by the permanent magnets and iron in the motor. According to B. G. King [4, 5], it is convenient to think of this as a friction torque. It can be modeled in much the same way as bearing solid friction torque, independent of the electromagnetic impressed torque, as long as the permanent magnets are not demagnetized significantly by the motor windings when current is applied.

The motor angular rate  $\dot{\theta}_M$  is input to the gearbox, as is the load angular rate reflected through the gears, to obtain the relative rate with respect to the gearbox input. This relative rate is amplified by the gear ratio to obtain the relative rate with respect to the output shaft. This rate is then integrated to get the angular deflection through the gearbox and output shaft. Most of the torque applied to the load is that transmitted through the box and shaft linear stiffness  $K$ . In parallel with the gear shaft stiffness is another solid friction model that takes into account the hysteresis friction of the gearbox. Torque is also applied to the load through this friction. The shape of a typical harmonic

drive-type gear and shaft stiffness and solid friction characteristic without backlash is shown in Figure 4. The case of backlash with hysteretic friction is more difficult to simulate, but some success has been attained by omitting the linear spring and using the friction slope model sketched in Figure 5. This gives the characteristic sketched in Figure 6 where the nominal stiffness is  $\sigma$  and the backlash region has a soft stiffness of  $\sigma_0$ .

To obtain experimental data on the static stiffness and solid friction hysteresis of the gearbox as shown in Figures 4 and 6, the angle measurements should be taken on the output shaft of the gearbox with the input shaft locked.

Completing the description of Figure 2, the sum of the linear stiffness torque and the gear solid friction torque less the load viscous and solid friction is what drives the load inertia. It is frequently found that the gear hysteretic friction provides a very significant amount of damping to the system.

Solid friction as well as magnetic "friction" is seen to enter the system in very significant ways. We shall show how each of these friction sources can be modeled using three friction model parameters (for each SFM). If a friction source or sources cannot be modeled accurately by a single SFM, multiple SFMs added in parallel can be used. In the following discussion, as an example, it is shown how ball bearing friction parameters are experimentally obtained. Test methods similar to those discussed here can be used to determine parameter values for the other solid friction sources. Raw and reduced test data for bearings are shown.

## II. SOLID FRICTION MODEL PARAMETERS

The mathematical model of solid friction is based on deriving the friction torque  $T(\dot{\theta}, t)$  or force  $F(x, t)$  from the time derivative of the friction that is a function of  $x$ , the angular or linear



relative displacement between system elements, and time  $t$ .

$$\frac{dF(x, t)}{dt} = \frac{dF(x)}{dx} \cdot \frac{dx}{dt} \quad (1)$$

Then, integrating Eq. (1) with respect to time  $t$

$$F(x, t) = \int \frac{dF(x)}{dx} \frac{dx}{dt} dt \quad (2)$$

The derivative of friction force with respect to deflection  $dF/dx$  is referred to as the friction slope function. It was found empirically [2] to be generally expressible as

$$\frac{dF}{dx} = \sigma \left| 1 - \frac{F}{F_c} \operatorname{sgn} \dot{x} \right|^i \cdot S \quad (3)$$

where

$$\operatorname{sgn} \dot{x} = \operatorname{sgn} \left( \frac{dx}{dt} \right) = \pm 1 \text{ for } \pm \text{ velocities, respectively}$$

$\sigma$  = rest stiffness parameter

$F_c$  = Coulomb friction level parameter

$i$  = SFM exponent parameter

$S$  = stabilizing factor, such as  $\left| \operatorname{sgn} \left( 1 - \frac{F}{F_c} \operatorname{sgn} \dot{x} \right) \right|$  for simulation work. If  $i = 1$ , then  $S = 1$  works.

The slope functions are defined for  $F/F_c$  between  $\pm 1$  and, although it is not theoretically possible for  $|F|$  to exceed  $F_c$ , use of a stabilizing factor  $S$  is required in some simulations to protect against instability that might occur as a result of factors such as computational roundoff.

The friction slope functions appear as shown in Figure 7 for various values of  $i$  for positive velocity  $\dot{x} > 0$ . The curves for negative velocity  $\dot{x} < 0$  are symmetric with the curves shown about the vertical axis  $F/F_c = 0$ .

Integration of Eq. (3) gives the general friction force-deflection function. In this paper, consideration is given to the cases where the SFM exponent parameter is set equal to 1.0 and 2.0 because the bearing friction data presented show that this parameter lies in this range and because there is an advantage in simulation and analysis using integer exponents. The case of  $i = 3/2$  approximates the best fit for the bearing data.

Integrating Eq. (3) with respect to  $x$  with  $\operatorname{sgn} \dot{x} = +1$  and using the initial condition  $F(x) = 0$  at  $x = 0$ , we get

$$\frac{F}{F_c} = 1 - \left[ 1 - (1 - i) \frac{x}{x_c} \right]^{1/(1 - i)} \quad (4)$$

where

$$x_c = \frac{F_c}{\sigma} \quad (5)$$

is the characteristic displacement or knee of the force-deflection curve. Note that if  $i < 1$ , Eq. (4) is valid for  $x/x_c < (1/(1 - i))$  and  $F/F_c = 1$  for  $x/x_c > (1/(1 - i))$ .

For  $i = 1$ :

$$\frac{F}{F_c} = \left( 1 - e^{-x/x_c} \right) \quad (6)$$

For  $i = 3/2$ :

$$\frac{F}{F_c} = 1 - \left( 1 + \frac{x}{2x_c} \right)^{-2} \quad (7)$$

For  $i = 2$ :

$$\frac{F}{F_c} = \frac{x}{x + x_c} \quad (8)$$

The knee parameter  $x_c$  can be regarded as an SFM parameter derivable from Eq. (5) if  $F_c$  and  $\sigma$  are determined. In any case, two of the three parameters in Eq. (5) need to be found from experimental data.

The shapes of the force-deflection functions given above for positive velocity  $\dot{x} > 0$  are evident in Figure 8. When the motion is reversed,  $\dot{x} < 0$  and the same shape curves are retraced in the negative direction. The SFM parameters are to be determined for the ball bearings from data that have the appearance of the curves in Figure 8.

### III. TEST METHOD

Basically, two test methods are available for use in determining the solid friction parameters: static force-displacement or torque-angular deflection tests, and second-order oscillation decay tests. In both methods, the phenomenon to be observed in the test is hysteresis. In the first method, the hysteresis loop is measured directly. In the second method, it is indirectly determined

by measuring the rate of damping of a spring-mass type of oscillator, as the rate of damping is related to the hysteretic energy dissipation per cycle. Due to time and space limitations, the second method is not discussed further; the reader is referred to References 2 or 3 for background theory. However, measurement methods are not treated in these references.

The test setup for the static test method for bearing tests that have been performed at The Aerospace Corporation is shown in Figure 9.

#### Bearing Test Fixture

The bearing test fixture is shown schematically in Figure 9 with two angular contact bearings back to back. A spacer between the two bearing outer races gives a load path through the outer races and assures separation of the inner races. The bearing inner races have a sliding fit to the fixture shaft, and are axially loaded by means of the inner race loading flange which has the preload applied via the springs between the sliding flanges. The preload is adjustable with the adjustment nut or the left end-bolt on the shaft that retains the left bearing inner race. Preload can be calibrated with deflection  $x$  or calculated if the spring constant of the springs is known. Generally, the surface friction with preload is sufficient to prevent relative rotation of the bearing inner races, preload flanges, springs, and shaft assembly. However, care was taken to assure that this was the case. Guide pins or other means can be employed between the preload flanges to assure free relative axial motion but prevent relative rotational motion between the flanges. The outer races were lightly fastened with small set screws to a mounting adapter that mounts on the head of the torque meter. A coupling on the inner race drive shaft was used to connect the bearing test fixture to the drive servo.

#### Torque Meter

The torque measuring device used was a McFadden Electronics Co. Servo Torque-Balance Reaction Dynamometer Model 117A. The mounting head or platform is air-bearing supported for axial and radial loads. When a torque is applied through the bearing test fixture to the head, a

small angular displacement occurs that is sensed by a feedback position transducer which sends a signal to a control and power electronics unit that supplies current to a torquer. The torquer output reacts against the input applied torque to provide a balance. The stiffness of this closed-loop servo torque meter was measured to be about 0.015 in-oz/arc-sec, or 0.28 ft-lb/deg, which was about an order of magnitude stiffer than the rest-stiffness of the bearing being tested. The torque meter has three ranges: 0 to 2, 0 to 20, and 0 to 200 in-oz. It was used on the 0 to 20 in-oz scale.

Meter accuracy was specified at  $\pm 2\%$  (of full scale) on each range with the threshold to be less than 0.001 in-oz. A nonlinearity was found to exist at null, and an unbalance weight was mounted on the head to cause a bias torque so that the bearing torque excursions operated in a linear region of the torque meter. In addition, the torque meter was indicated in a test to exhibit a torque reading output hysteresis change of 0.1 in-oz when the direction of motion was reversed. These error sources were considered negligible for the bearings tested.

#### Drive Servo

The drive servomotor was used to drive the inner races of the ball bearings in an oscillatory manner in order to trace out a hysteresis loop similar to one of those shown in Figure 8. The input to the servo was a triangular waveform voltage from an electronic function generator set at 0.05 Hz. This frequency was well below the bandwidth of the torque meter ( $\sim 10$  Hz) and x-y plotter used to record the data, and it gave angular rates well below those where viscous friction effects would become troublesome. The triangular waveform was found to give better results than a sine waveform because slight noise in the system at the near-zero angular rate part of the sine wave cycle would act as jitter, giving short rate reversal cycles that would jog the torque toward zero. The sudden rate reversal of the triangular waveform minimizes this effect because the forward and reverse rates are maintained high relative to the noise rates except at the instant of rate reversal.

The motor used was an Inland D. C. brush-type torquer with a stall torque of 7.5 ft-lb. The

power amplifier was also an Inland unit. A Baldwin 18-bit incremental encoder was mounted on the motor and coupled directly to the motor drive shaft. An in-house designed and built digital-to-analog (D/A) converter processed the encoder output signal, and its output was fed to a difference amplifier with compensation circuitry. The 12-bit D/A converter defined the range and quantization bit resolution values available for the drive servo as shown in Table I. The  $\pm 11.25$  deg range with the 0.011-deg quantization bit resolution was used for this test. The drive servo position hysteresis for small excursions was less than about 0.001 deg. The bandwidth of the drive servo was about 10 Hz, and the short term noise level was of the same order of magnitude as the position hysteresis, i.e., 0.001 deg. The output of the drive servo was used to drive the x-axis of an x-y recorder, and the torque meter output was used to drive the y-axis.

The duplex bearing pair tested was a Barden 104H, Class 5, with a bore diameter of 20 mm, a ball diameter of 0.25 in., and race width of 12 mm. The bearings had been used in a Bendix Corporation test fixture and indicated significant torque noise as shown by the torque waviness imposed on the hysteresis loop in Figure 10. Inspection of the bearings confirmed the suspicion of worn balls and races, so a new set was obtained. Test runs were made on the new bearings for preloads of 6, 12, 18, 24, 30, and 36 lb. Figure 11 is a typical hysteresis trace obtained with the new bearings for the same preload of 24 lb used for Figure 10.

#### 11. DATA ANALYSIS

For purposes of analyzing the hysteresis data, it is advantageous to define

$$f = F_c - F \quad (9)$$

and

$$x' = x - x(-F_c) \quad (10)$$

for  $\dot{x} > 0$  (or  $f = F - F_c$  for  $\dot{x} < 0$ ). Either the increasing or decreasing half of the hysteresis loop or both can be analyzed. The increasing half in Figure 11 is shown with the  $f$  and  $x'$  axes labeled in graph paper units where the  $x' = 0$  axis passes through the rate reversal point. In terms of these

variables and assuming that  $f = 2F_c$  at the rate reversal point when  $x' = 0$  and that  $\dot{x} < 0$ , Eqs. (3), (4), (6), and (8) can be written respectively as

For  $i \geq 0$ :

$$\frac{df}{dx'} = \frac{F_c}{x_c} \left( \frac{f}{F_c} \right)^i \quad (11)$$

$$\frac{f}{F_c} = \left[ 2^{1-i} - (1-i) \frac{x'}{x_c} \right]^{1/(1-i)} \quad (12)$$

For  $i = 1$ :

$$\frac{f}{F_c} = 2e^{-x'/x_c} \quad (13)$$

For  $i = 2$ :

$$\frac{F_c}{f} = \frac{x'}{x_c} + 1/2 \quad (14)$$

Equation (12) can be used in data analysis parameter estimation programs, but it is nonlinear and is not readily put into a linear form by simple changes of variables.

The quantities  $df/dx'$ ,  $f/F_c$ , and  $F_c/f$  on the left side of their respective equation can be considered as dependent variables and the variables  $f$  and  $x'$  on the right side as independent variables. The graph of Eq. (11) plotted as  $df/dx'$  versus  $f$  on the log-log graph paper is linear as is the plot of  $f$  versus  $x'$  for Eq. (13) on semi-log graph paper and the plot of  $1/f$  versus  $x'$  for Eq. (14) on rectangular graph paper. Thus, the least-squares fit linear regression method can be applied to the  $f$ ,  $x'$  data pairs for points on the hysteresis curves. Computer programs are available on large and small computers to analyze data by this method. Other computer programs can be used that fit nonlinear functions such as Eq. (12) to a set of data, but these programs generally are available only on large computers. The programmable Hewlett-Packard hand-held calculators can be utilized to perform the linear regression analysis, and the HP 67 and HP 97 units have curve-fitting program cards that can be used to fit data to straight lines (Eq. [14]), exponential curves (Eq. [13]), logarithmic curves, and power curves (Eq. [11]). Because of its convenience and simplicity, the HP 67 curve-fitting program was used in analyzing the bearing test data. A description of the program is given in the

HP 67 "Standard Pac." Some simple preprocessing of the data to calculate  $df/dx$  and  $1/f$  was necessary before it could be used in the standard curve-fitting program. The program effectively outputs the parameters  $i$  and  $x_c$  for Eq. (11) and  $x_c$  for Eqs. (13) and (14). The parameter  $F_c$  is initially estimated by inspection of the hysteresis curve and is specified by the location of the  $f = 0$  and  $x' = 0$  axes on the  $x$ - $y$  test data plots.

## V. RESULTS AND CONCLUSIONS

Test data for the "running" or Coulomb friction were readily obtained by visually estimating the horizontal asymptotes. Results are shown in Figure 12. Both old and new bearing running friction levels were effectively taken as the average of the near asymptotic wavy torque level. The envelope of the old bearing asymptotic wave peaks was only 5 to 15% higher than the average value. Thus, it appears from this data that the wear process increases noise torque but decreases running friction in the mid to high preload range. The friction of the new bearings at the high preload of 36 lb appeared at first to be an outlying data point. However, the old bearing data show the same characteristic of suddenly increasing at 36 lb preload. A 40-lb preload is considered a heavy preload by the manufacturer.

Results of the curve-fitting data analysis are presented in Table II for the new bearings. The characteristic angular displacement  $x_c$  was found from the plots by drawing the tangent or the rest slope  $\sigma = F_c/x_c$  to the curves at  $F = 0$ , and is designated with the heading  $x_c = F_c/\sigma$ . The curve fit program was used to find the parameters  $i$  and  $x_c$  from the power fit for Eq. (11) as well as the parameter  $x_c$  from the exponential fit for Eq. (13) and from the linear fit for Eq. (14). Results are listed in the table with the coefficient of determination  $r^2$ , which indicates goodness of fit, and the friction range where the fits are good,  $f_{LIM} < f < 2F_c$ . The curve fits deviate from the experimental curves for  $f$  values below  $f_{LIM}$ .

It seemed important for each curve fit to have approximately the correct value of rest slope  $\sigma$ , and so the data for  $f < f_{LIM}$  were deleted because the value of  $x_c$  determined from the fit deviated excessively from the rest slope value if that data

were included. Thus, even though the  $i = 1$  and  $i = 2$  fits have better coefficients of determination than the power curve fit, they will not fit the data over as wide a range and still have the correct rest slope. With this in mind, it is observed that values of  $x_c$  for the power fit curves are about 15% below the graphical  $x_c$ ,  $i = 1$  fit curves have values for  $x_c$  slightly higher than the graphical values, and the  $i = 2$  fit curves have values for  $x_c$  that are about 50% below the graphical values.

It is concluded, as a result of this testing, that the  $i = 2$  fit curves are not as accurate as the  $i = 1$  and  $i \approx 1.5$  fit curves. A useful observation is that the  $i = 1$  fit curves give good results over about 95% of the range of friction change from  $-F_c$  to  $+F_c$ . They also give a good fit for the rest slope.

It is important to observe that the value of  $x_c$  is approximately constant and independent of preload.

Another important conclusion that can be drawn from these data is that the SFM exponent parameter  $i$  is approximately constant and has an average value of about 1.5.

## REFERENCES

1. P. R. Dahl, A Solid Friction Model, TOR-0158(3107-18)-1, The Aerospace Corporation, El Segundo, Calif. (May 1968).
2. P. R. Dahl, "Solid Friction Damping of Spacecraft Oscillations," Paper No. 75-1104, Paper presented at the AIAA Guidance and Control Conference, Boston, Mass., August 1975.
3. P. R. Dahl, "Solid Friction Damping of Mechanical Vibrations," AIAA Journal, **14** (12), 1675-1682 (December 1976).
4. B. G. King, Ball Bros. Research Corp., Boulder, Colo., Private correspondence, June 1976.
5. B. G. King, "Simulation of D.C. Torque Motor Magnetic Hysteresis and Cogging Effects," Paper to be presented at the Sixth Annual Symposium on Incremental Motion Control Systems and Devices, University of Illinois, Urbana-Champaign, Illinois, May 1977.

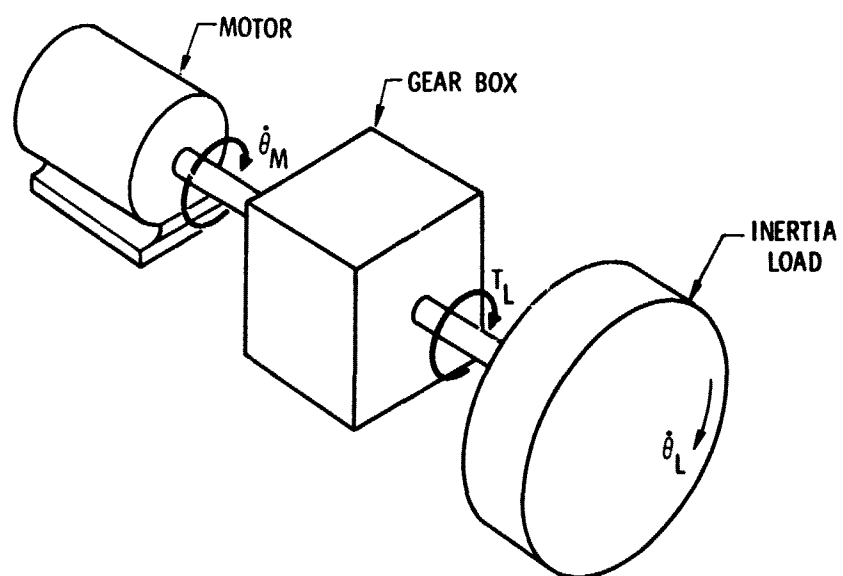


Figure 1. Motor/Gear Box/Load System

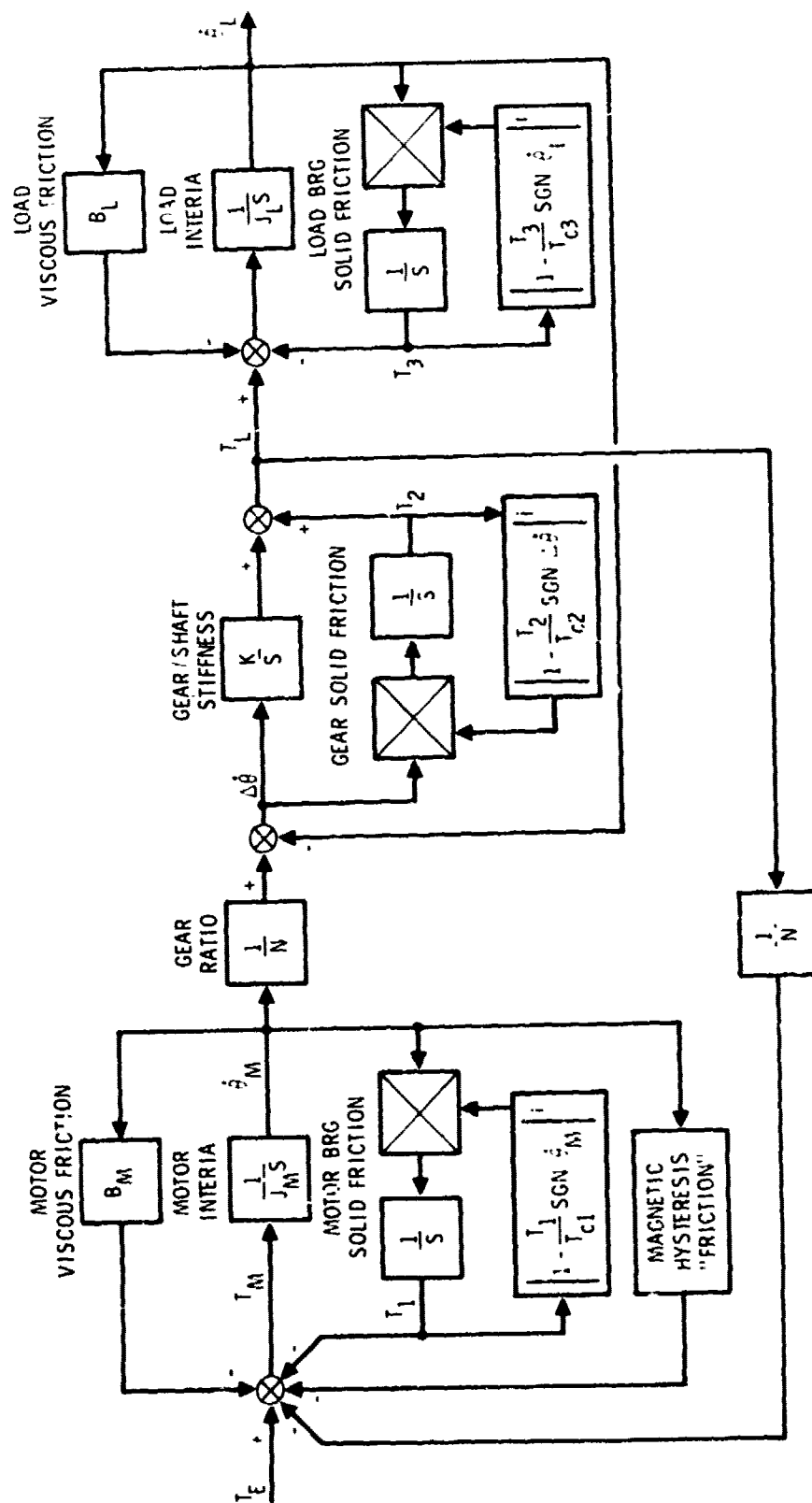


Figure 2. System Diagram

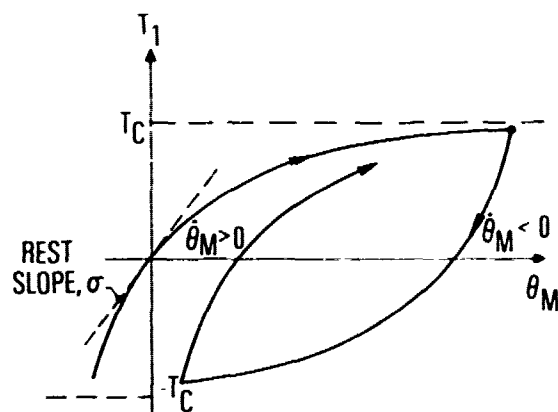


Figure 3. Solid Friction Behavior

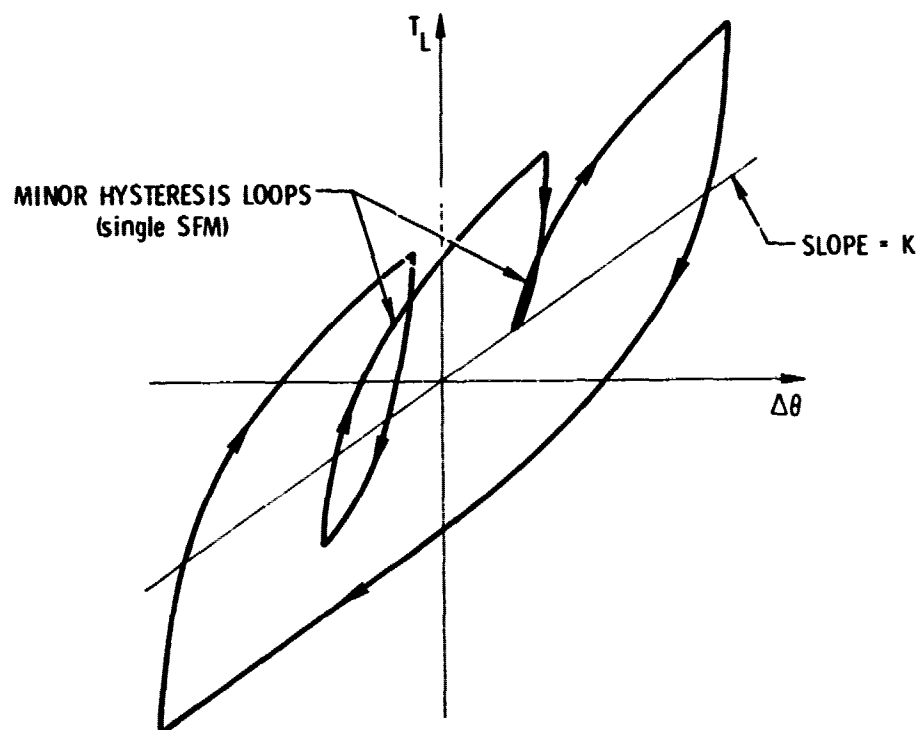


Figure 4. Gear-Shaft Stiffness with Hysteresis  
(as Measured at Output Shaft)

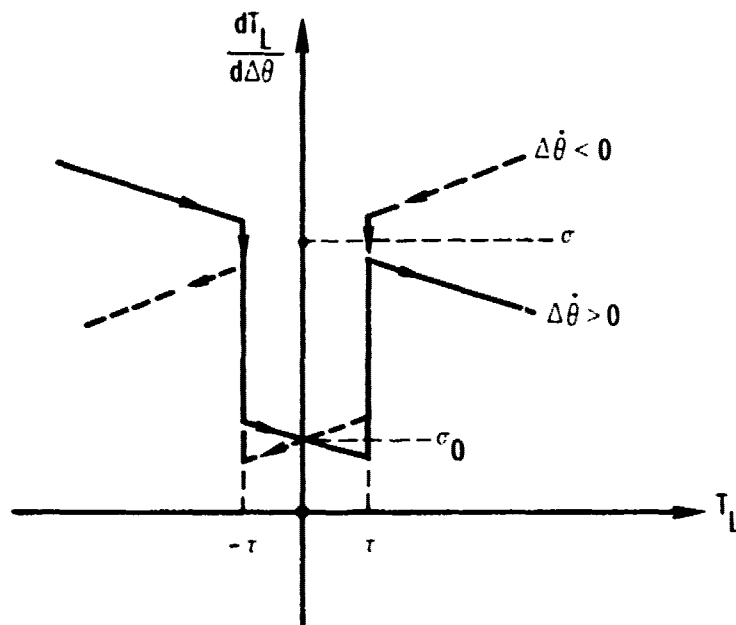


Figure 5. Friction Slope Model for Gear-Shaft Stiffness, Hysteresis, and Backlash



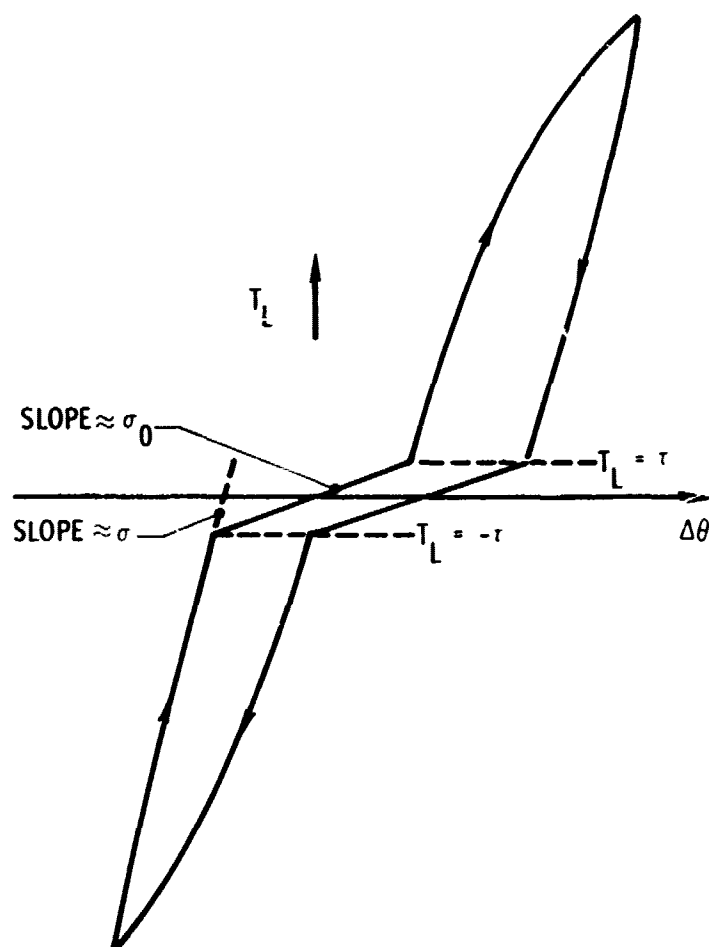


Figure 6. Gear-Shaft Stiffness with Hysteresis and Backlash

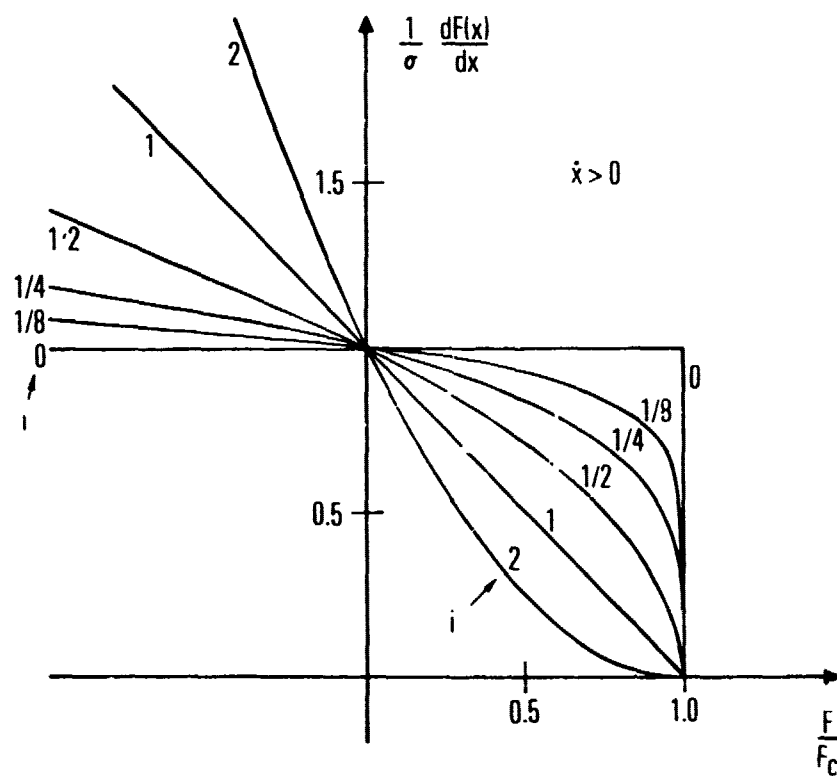


Figure 7. Friction Slope Functions

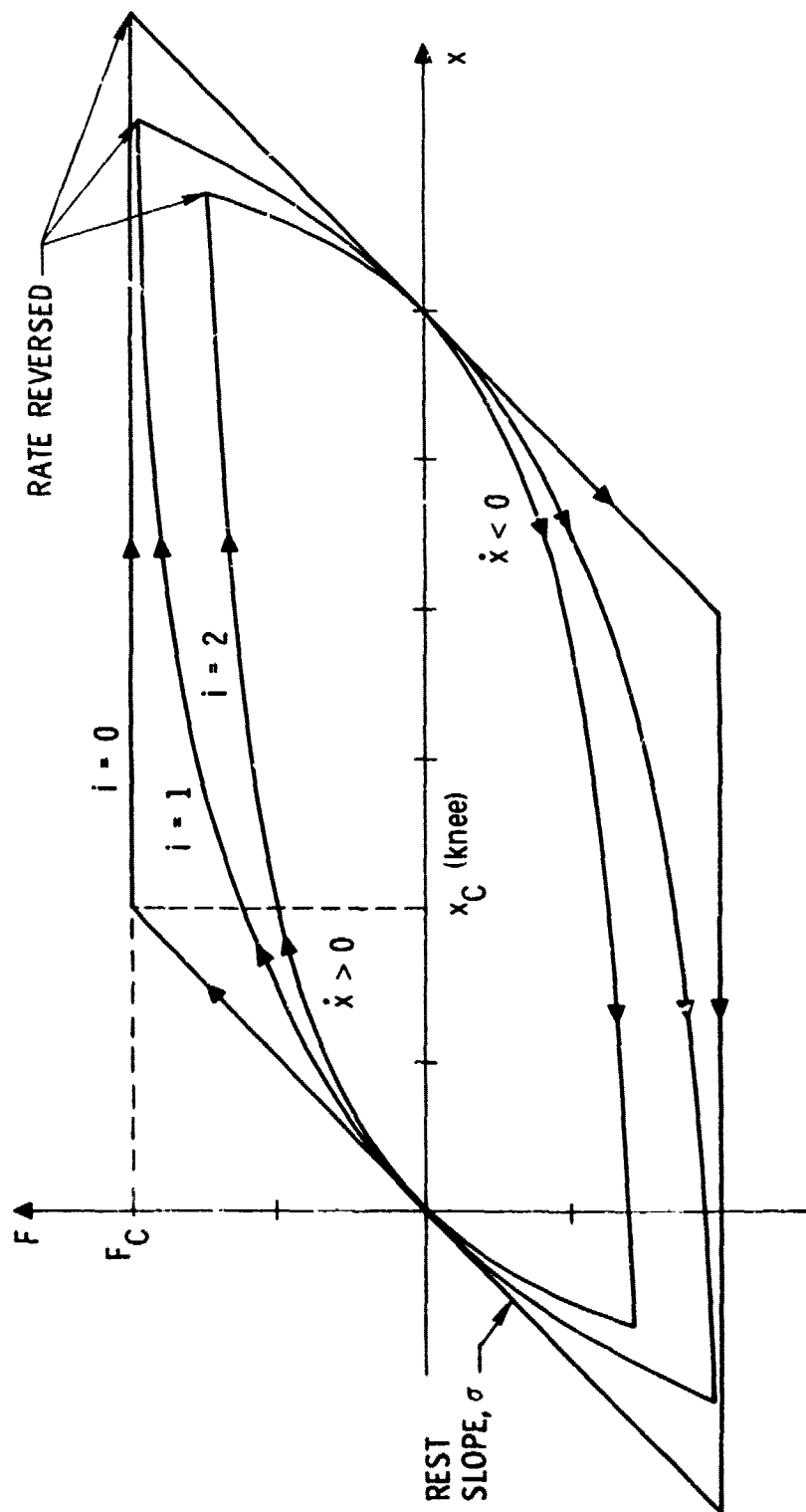


Figure 3. Force Deflection Hysteresis Loops

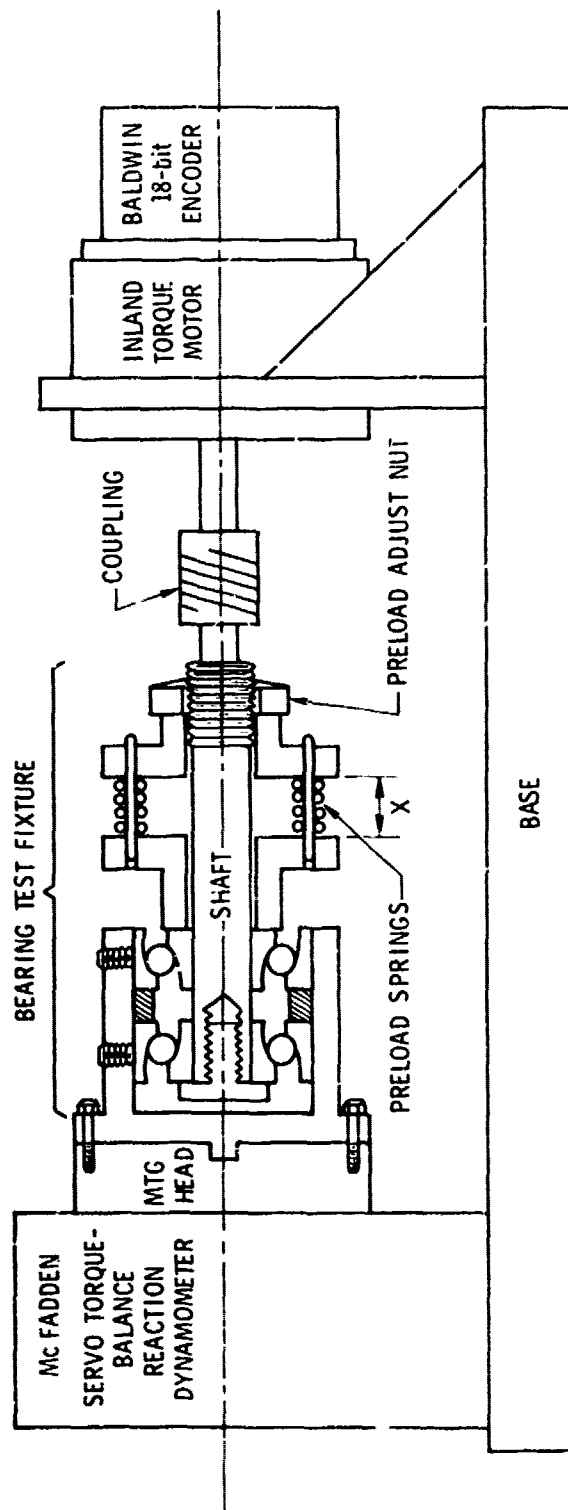


Figure 9. Bearing Static Torque-Deflection Test Setup

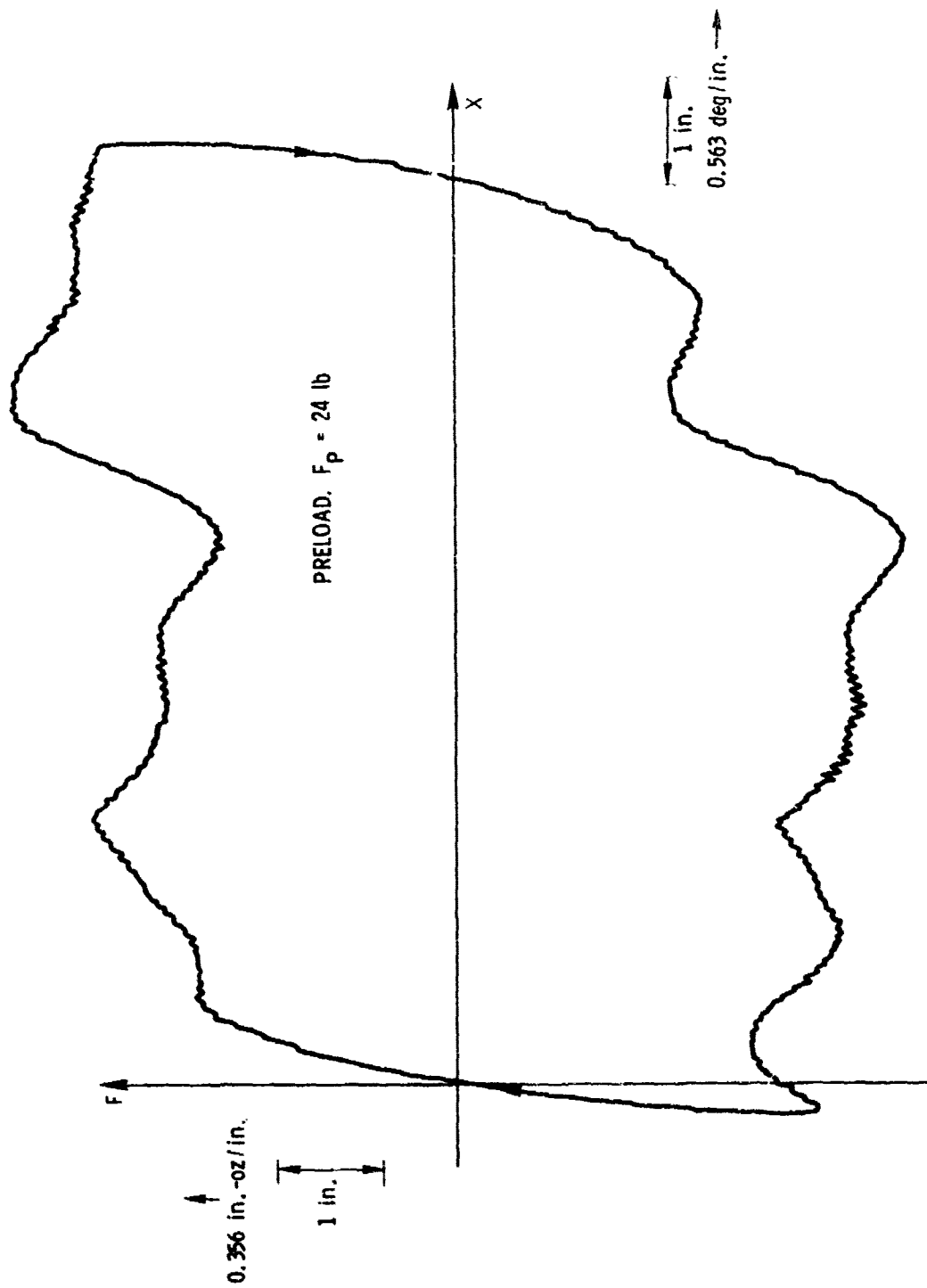


Figure 10. Old Bearing Hysteresis Loop

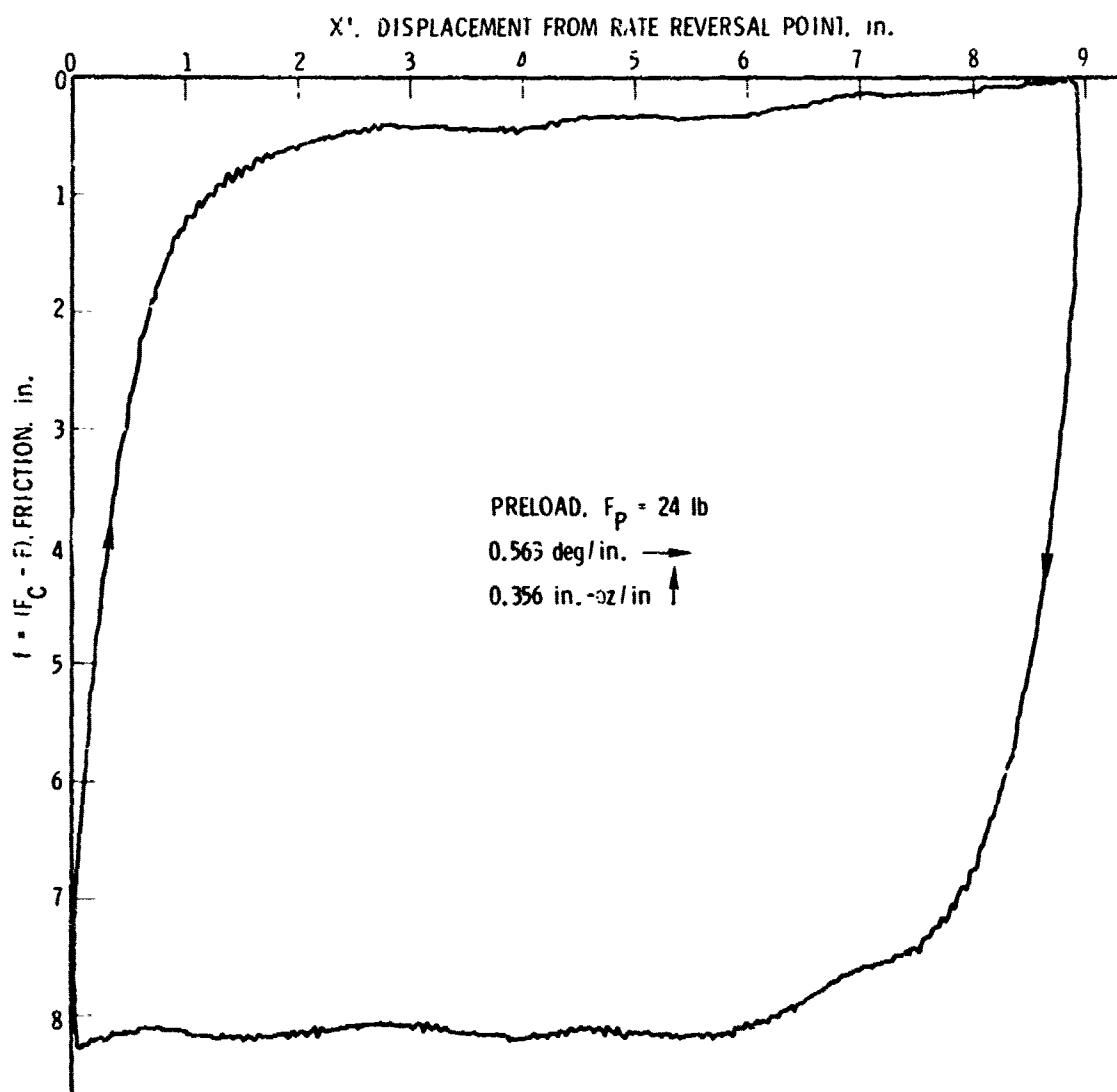


Figure 11. New Bearing Hysteresis Loop

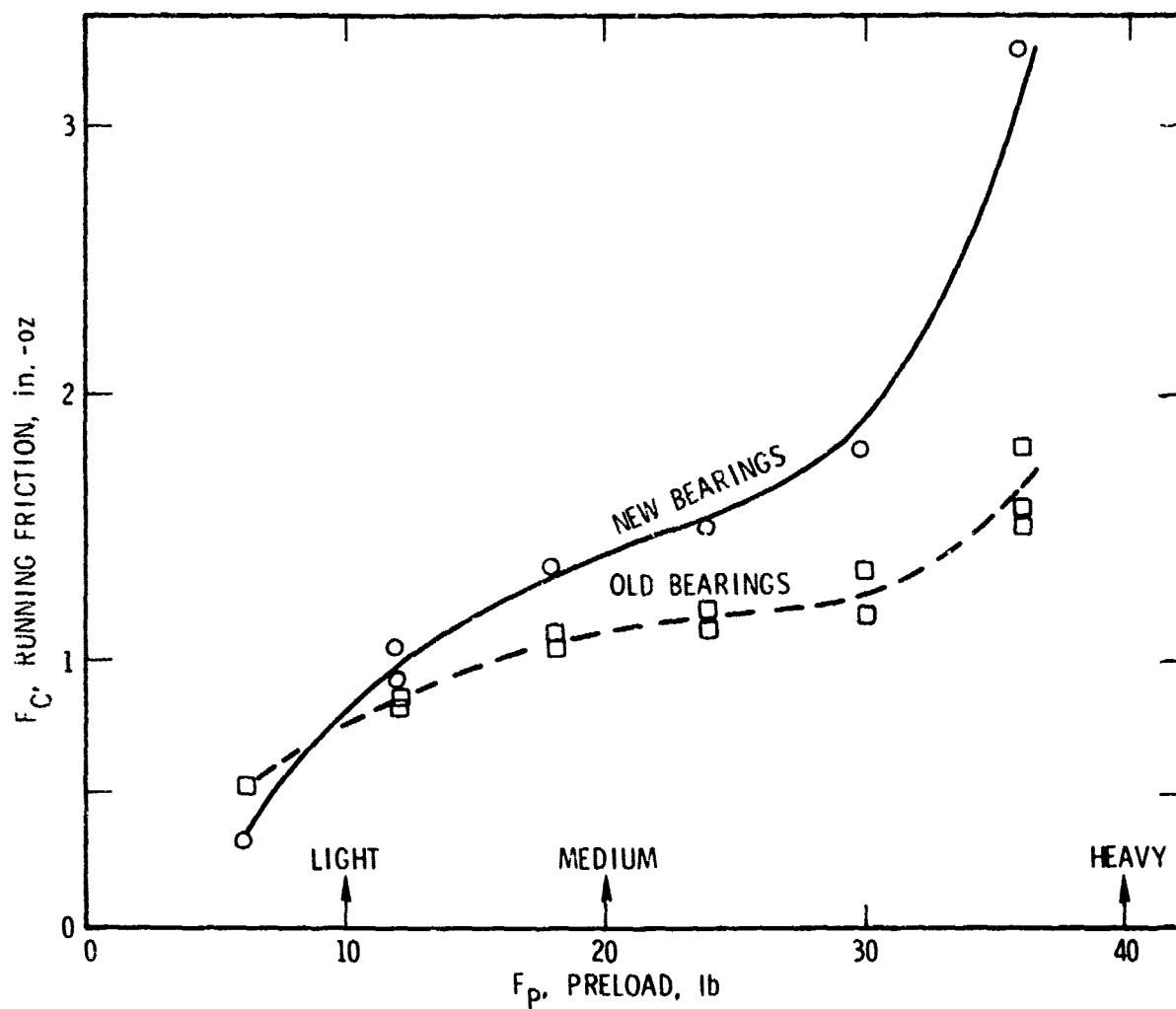


Figure 12. Running Friction versus Preload

Table I. Drive Servo Range and Resolution

Range (deg)	Quantization Bit Resolution (deg)	Scale Factor (V/deg)
$\pm 0.703$	0.00069	14.222
$\pm 2.81$	0.0027	3.555
$\pm 11.25$	0.0110	0.8888
$\pm 45.0$	0.044	0.2222
$\pm 180.0$	0.176	0.05555



